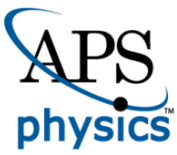

Asymptotically optimal probes for noisy interferometry via quantum annealing to criticality

Gabriel A. Durkin

Phys. Rev. A **94**, 043821 — Published 13 October 2016

DOI: 10.1103/PhysRevA.94.043821

Asymptotically-Optimal Probes for Noisy Interferometry via Quantum Annealing to Criticality.

Gabriel A. Durkin[1, 2, *]

[1] *Berkeley Center for Quantum Information and Computation, University of California, Berkeley, CA 94720*
[2] *Peliquan Technologies, 950 Franklin St., Suite 1, San Francisco, CA 94109*

Quantum annealing is explored as a resource for quantum information beyond solution of classical combinatorial problems. Envisaged as a generator of robust interferometric probes, we examine a Hamiltonian of $N >> 1$ uniformly-coupled spins subject to a transverse magnetic field. The discrete many-body problem is mapped onto dynamics of a single one-dimensional particle in a continuous potential. This reveals all the qualitative features of the ground state beyond typical mean-field or large classical spin models. It illustrates explicitly a graceful warping from an entangled unimodal to bi-modal ground state in the phase transition region. The transitional 'Goldilocks' probe has a component distribution of width $N^{2/3}$ and exhibits characteristics for enhanced phase estimation in a decoherent environment. In the presence of realistic local noise and collective dephasing, we find this probe state asymptotically saturates ultimate precision bounds calculated previously. By reducing the transverse field adiabatically, the Goldilocks probe is prepared in advance of the minimum gap bottleneck, allowing the annealing schedule to be terminated 'early'. Adiabatic time complexity of probe preparation is shown to be linear in N.

PACS numbers: 42.50.-p,42.50.St,06.20.Dk

I. INTRODUCTION

In quantum metrology[1, 2] we often seek to estimate a continuous time-like parameter associated with unitary evolution. Even without a direct Hermitian observable for time or phase, one can determine bounds on the mean-squared error of estimated values as a function of N, the number of qubits, particles, spins or photons involved in the measurement. The lowest bounds are associated with initializing the instrument in a particular entangled quantum configuration of the N qubits, known as a 'probe' state. Without entanglement, the performance cannot exceed the precision resulting from sending qubits through the instrument one at a time. Large spin and mean-field models used to describe many-body systems typically ignore entanglement altogether. Curiously, in a noisy setting the most entangled states do not offer the greatest precision [3].

In the noiseless case, it has been known for some time that the optimal configuration of the N qubits is the NOON[4, 5] or GHZ [6] state. This is an equal superposition of the two extremal eigenstates of the phase-encoding Hamiltonian. Subsequently, however, we have come to understand that this state offers sub-optimal performance in the presence of realistic noise or decoherence, and recent work has unveiled a new family of optimal probe states for noisy metrology [7].

Unfortunately, these new probes brings with them the challenge of how they might be generated. The asymptotic analysis that uncovered the optimal states indicates also that, for any large-N probes, there will be a large precision penalty for those with discontinuities in the distribution of probe components. (This is the case with the NOON/GHZ state.). For a spin Hamiltonian like $\hat{J}_z$ associated with phase or frequency estimation, optimal probes typically inhabit the fully-symmetric subspace of largest overall spin $j = N/2$. For $N \gg 1$, optimality is achieved by a smooth unimodal distribution of spin projection amplitudes $\psi_m = \langle m|\psi\rangle$; for most physically-relevant noise types this distribution profile matches the ground state waveform for a one-dimensional particle trapped between two repulsive Coulomb sources[7]. The optimal distribution width $\Delta\hat{J}_z$ is dependent on the noise strength and is typically wider than $\sqrt{N}$, i.e. it is anti-squeezed in the z-direction. Had the optimal probe this 'square-root' width, it would be easily produced by rotating an N -spin coherent state (all spins up) by $\pi/2$ around the y-axis via an optical pulse. This state is a simple product state of the component spins – creating 'wider' optimal probes introduces partial, or 'just the right amount' of entanglement to the ensemble.

In this paper, we explore techniques to generate such 'Goldilocks' quantum probes, balancing sensitivity against robustness.

II. HAMILTONIAN FOR PROBE PREPARATION

Bearing in mind the ideal characteristics above, one might start to imagine how such broad, smooth, unimodal probe-state distributions could be engineered. To this end, one of the simplest non-trivial quantum systems that can be investigated is one with an equal $\hat{\sigma}_z^{(1)}\hat{\sigma}_z^{(2)}$ coupling between all pairs of qubits in the presence of a transverse field. The field strength increases monotonically with an 'annealing' parameter Γ:

$$\hat{H} = -\Gamma\frac{\hat{J}_x}{j} - (1-\Gamma)\frac{\hat{J}_z^2}{j^2} \tag{1}$$

where $2\hat{J}_z = \hat{\sigma}_z^{(1)} + \hat{\sigma}_z^{(2)} + \hat{\sigma}_z^{(3)} + \ldots$ In this scaled form, $|\langle\hat{H}\rangle| \leq 1$; so $j\hat{H}$ corresponds to actual energies. This system exhibits a continuous quantum phase transition, as follows. Initializing the system in the ground state of a strong transverse field $\Gamma \lesssim 1$, all spins are aligned with the x-axis (this is the coherent spin state discussed in the introduction).

*Electronic address: Gabriel.Durkin@qubit.org

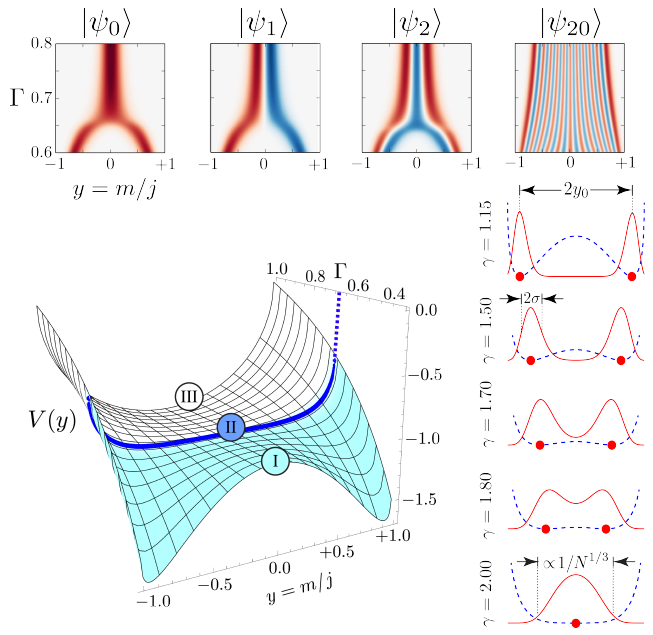

FIG. 1: Pseudo-potential $V(y)$ from eqn.(6) that results in the large N limit from mapping the quadratic spin Hamltonian onto a 1-D particle in a potential well. The evolution from a single well in Region III through a critical Region II to a double-well in Region I is apparent as the transverse field is decreased, or equivalently, as the annealing parameter Γ is swept from 1 to 0 (large inset). In Region III where the transverse field is strongest, the ground state will be all spins aligned with the field along the x-axis. In the variable y, this is a Gaussian state of width $1/\sqrt{N}$. Gaussian states are the ground state of a quadratic potential. At $\Gamma = 1$, however, the pseudo-potential of the inset figure looks like a semi-circle. There is effectively no disparity because the ground state is very narrow for large N, and has very low probability away from $y = 0$; within this locale $V(y)$ also looks quadratic. The dark (blue) contour in Region II indicates the quartic form of the potential at the critical point, where the annealing parameter $\Gamma_c = 2/3$ or $\gamma_c = \Gamma_c/(1-\Gamma_c) = 2$. For $N = 100$, the right-hand-side vertical sequence shows the ground state of the original spin Hamiltonian (red unbroken peaks) overlaid by the pseudo-potential (blue dashed curve), with potential minima indicated by dots. For an $N = 200$ ensemble, eigenstates $|\psi_n\rangle$ with $n \in \{0, 1, 2, 20\}$ pass through the critical region in the uppermost four panels; lower energy states exhibit a *pitchfork bifurcation* associated with the phase transition, but the highly-excited $n = 20$ state barely registers the structure of the potential far below. (Positive amplitudes in red, negative in blue.)

Then, as the field is gradually attenuated, the parameter Γ decreases to a critical value $\Gamma_c = 2/3$, at which point the ground state warps *continuously* into a qualitatively different bimodal NOON-like profile (exactly a NOON state when $\Gamma = 0$). If the annealing proceeds slowly enough, the spins will remain in the instantaneous ground state at all times; this is adiabatic passage.

How realistic are such annealing dynamics? Quadratic terms like $\hat{J}_z^2$ appear frequently in models of two-mode Bose-Einstein condensates[8, 9] (BEC) , describing collisional processes. The two modes may correspond to a single condensate in a double-well potential, or a mixture of atoms in two distinct hyperfine states in a single potential. One of the earliest proposals for generating the spin-spin couplings was introduced in the context of ion traps illuminated by two laser fields[10]. This Hamiltonian is also referred to as the isotropic *Lipkin-Meshkov-Glick* (LMG) model [11], an infininte-range Ising model with uniform couplings. The LMG model can provide an effective description of quantum gases with long range interactions[12]. In terms of metrology, the precision offered by some Ising models in a decoherence-free setting was given careful examination recently in Ref.13.

Similarities exist with the dynamics of of a single-mode oscillator (optical field in a cavity), coupled adiabatically to a collection of spins or atoms via the Dicke Hamiltonian [14], where the coherence length of the field is much larger than the physical extent of the particle ensemble. The single-mode field introduces an effective ferromagnetic spin-spin coupling. The intensity of light emitted into the Dicke super-radiant phase can also be utilized for high-precision thermometry [15] for probes prepared in close proximity to the critical point.

It is not our goal to measure the temperature, evolution time, transverse field or any other 'native' property of this system. Rather, the objective is to utilize the annealing dynamics as a resource for engineering robust high-precision probes for interferometry in noisy environments.

The Hamiltonian of eqn.(1) has been considered previously for interferometry in works that suggest that it is a good source of squeezing and, as such, should lead to better precision. Those prior works[16, 17], however, did not describe the dynamics through the critical region, where we believe maximum precision is possible. We now know[7] that the extent of probe squeezing is not a good quantification of precision in a noisy interferometer (the most squeezed input states may be some of the most fragile). We will later show that for this scheme, ultimate precision is *only* attained by critically-annealed probes.

III. MAPPING ONTO A PARTICLE IN A POTENTIAL

To capture fully the behaviour of this discrete spin system at large N throughout the phase transition (and determine if it has appropriate properties for noisy interferometry), we map it onto a continuous particle problem.

The idea of mapping a quadratic spin Hamiltonian in a transverse field onto a one-dimensional particle in a potential is not a new one; many examples exist in the literature [18–22]. A typical approach involves 'bosonization' of the spin operators into combinations of $\hat{a}$ and $\hat{a}^\dagger$, using either Holstein-Primakoff [23] or Villain [24] transformations. Then, after identifying quadratures $\hat{x} = (\hat{a}+\hat{a}^\dagger)/2$ and $\hat{p} = -i(\hat{a}-\hat{a}^\dagger)/2$, an operator differential equation in x and $\hat{p} = -id/dx$ is produced that, after some approximations, may resemble a Schrödinger equation. (One may choose to linearize the boson operators about the mean-field direction.) Limitations of a truncated Holstein-Primakoff description of the LMG model we consider here are discussed in Ref.[25].

To understand the behaviour near the critical point, the mapping must remain faithful to the original discrete spin dy-

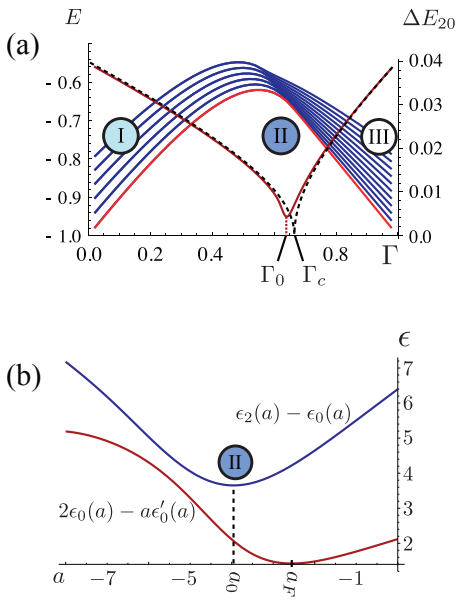

FIG. 2: In upper plot (a) energy levels E_n for $n \in [0, 11]$ (left vertical axis, multiple curve sequence with maxima near Γ_c) and ground-state energy gap $\Delta E_{20} = E_2 - E_0$ (curve plotted with minimum at Γ_0, right vertical axes) for an $N = 100$ spin ensemble as the annealing parameter Γ is swept from 0 to 1 through the location of the minimum gap Γ_0 and the critical Γ_c where the phase transition occurs in the thermodynamic limit, $N \gg 1$. In Regions I and III, energy levels are uniformly distributed $\Delta E \propto 1/j$, although in Region I neighbouring even and odd numbered levels pair up; only exponentially small gaps separate them. Dashed curve indicates the energy gap in the thermodynamic limit of eqn.(14). Plot (b) shows Region II landmarks: Numerical results in the scale-free system are shown for the precision penalty factor (lower red curve) from eqn.(18), and ground state gap (upper blue curve) near the critical point $a = 0$ (or $\Gamma = 2/3$). It is observed that a_F, the point of maximum precision is to the right of the minimum gap a_0, and therefore $\Gamma_F > \Gamma_0$, also. Any annealing schedule from strong to weak transverse field will reach the point of highest precision before it encounters the minimum gap.

namics, both qualitatively and quantitatively (to leading order, when finite size effects are considered). As a caveat, it is admitted that certain subtle phenomena may not be captured, e.g. exponentially small ground-state splitting that occurs for a weak transverse field. This requires precision calculation of small probability 'tails' deep inside the barrier dividing a double potential well [26], e.g. region I of FIG.1. Luckily, interferometric precision is quantified largely by the bulk probabilities of the probe-state concentrated at the bottom of the potential wells; any evanescent amplitude in the forbidden region makes an exponentially subordinate contribution.

Using notation $\hat{J}_z|m\rangle = m|m\rangle$ for eigenstates of $\hat{J}_z$ labelled by magnetic quantum numbers $m \in \{-j, -j+1, \ldots, +j\}$ one may represent the quantum ground state as a vector of amplitudes ψ_m in the $|m\rangle$ basis,

$$|\psi_0\rangle = \sum_{m=-j}^{+j} \psi_m |m\rangle \tag{2}$$

Take the overlap $\langle m|\hat{H}|\psi_0\rangle$ in the eigen-equation as

$$-\langle m| \left\{ \Gamma \frac{\hat{J}_x}{j} + (1-\Gamma)\frac{\hat{J}_z^2}{j^2} \right\} |\psi_0\rangle = E_0 \langle m|\psi_0\rangle \ . \tag{3}$$

Remembering $\langle m|\psi_0\rangle = \psi_m$ and $\langle m\pm1|\psi_0\rangle = \psi_{m\pm1}$ and the definition in terms of ladder operators, $\hat{J}_x = (\hat{J}^{(+)} + \hat{J}^{(-)})/2$ where $\hat{J}^{(\pm)}|m\rangle = \sqrt{j^2 - m^2 + j \mp m}|m \pm 1\rangle$, let's introduce the annealing 'ratio', $\gamma = \Gamma/(1-\Gamma)$. Assuming $j \gg 1$, one can transform into a continuous variable picture (effectively the reverse technique to solving differential equations numerically by discretizing variables). We assume a small parameter $\delta = 1/j$ for asymptotic expansions, and introduce a continuous variable $y = m/j \in [-1, 1]$, mapping $\psi_m \mapsto \psi(y)$ and $\psi_{m\pm1} \mapsto \psi(y \pm \delta)$. Assuming features change smoothly on a scale $\sim \delta$ one may define derivatives:

$$\frac{\psi(y+\delta) - \psi(y-\delta)}{2\delta} \mapsto \frac{d\psi}{dy} \tag{4a}$$

$$\frac{\psi(y+\delta) + \psi(y-\delta) - 2\psi(y)}{\delta^2} \mapsto \frac{d^2\psi}{dy^2} \tag{4b}$$

Having transformed $\langle m|\hat{H}|\psi\rangle$ from a difference equation to a differential equation, the eigen-equation becomes a Schrödinger equation for a one-dimensional particle of variable mass in a pseudo-potential, as follows:

$$\left[\frac{1}{2}\hat{P}\hat{M}^{-1}\hat{P} - \hat{M}^{-1} - \frac{y^2}{\gamma} \right] \psi(y) = \frac{E_0}{\Gamma}\psi(y) \ , \tag{5}$$

given an inverse mass operator, $\hat{M}^{-1}(y) = \sqrt{1-y^2} + \frac{\delta}{2}\frac{1}{\sqrt{1-y^2}}$, and a momentum operator $\hat{P} = -i\delta\frac{d}{dy}$. When solved numerically, the eigenstates of this continuous differential equation map faithfully onto the probability amplitudes for the original quadratic spin problem. See FIG.8 in the appendix. Variable-mass Schrodinger equations have been tackled analytically previously, e.g. in Refs.27, 28.

Written as $\hat{P}\hat{M}^{-1}\hat{P}/2$ the kinetic energy operator takes the form of a manifestly Hermitian operator. The pseudo-potential is

$$V(y) = -\frac{y^2}{\gamma} - \sqrt{1-y^2} - \frac{\delta}{2}\frac{1}{\sqrt{1-y^2}} \ . \tag{6}$$

This potential is depicted for $\delta \ll 1$, i.e. $N \gg 1$, in FIG.1, taking the form of either a single or double well. For large N, the distribution will be concentrated at the bottom of these wells at y_0 (red dots in FIG.1), and one may make the simplification in the kinetic term: $\hat{M}^{-1}(y) \mapsto 1/M(y_0) = 1/M_\gamma$ where y_0 will be a function of the parameter γ.

As such, when $\delta \ll 1$ the Hamiltonian becomes

$$\hat{H} \mapsto \Gamma \left(\frac{\hat{P}^2}{2M_\gamma} - \frac{y^2}{\gamma} - \sqrt{1-y^2} \right) \ . \tag{7}$$

IV. CHARACTERISTIC ENERGY AND LENGTH SCALES AT CRITICAL POINT

Our hope is that near criticality, (bifurcation point of FIG.1) the ground state may have properties that make it a promising candidate for noisy interferometry. Interestingly, the potential terms quadratic in y can be made to vanish at a critical transverse field Γ_c. For states strongly concentrated near $y = 0$, expand $V(y)$ as a Taylor series.

$$V(y) \approx -1 + \frac{y^2}{2}\left(1 - \frac{2}{\gamma}\right) + \frac{y^4}{8}\,. \tag{8}$$

It is seen that the leading order term of $V(y) \approx y^4/8$ near $\gamma_c = 2$, ($\Gamma_c = 2/3$), when $\delta \ll 1$. One might expect the quartic ground state also to have a distribution of width scaling greater than $\sqrt{N}$ and, as such, may be a robust probe in noisy conditions. The width can be checked by employing a Symanzik scaling argument. (A similar approach was used in Ref.14 to recover finite size corrections to the critical exponents at exactly $\gamma_c = 2$.) Due to the reflection symmetry about $y = 0$ the inverse mass $1/M_\gamma$ has a minimum value $1/M_2$ there and its first derivatives vanish. Again, expand $V(y)$ to the fourth power and the Schrödinger equation in the vicinity of $y = 0$ becomes

$$\left[-\frac{d^2}{dy^2} + \nu y^2 + g y^4\right]\psi_n = \tilde{E}_n \psi_n \tag{9}$$

where $\tilde{E}_n = \left(\frac{E_n M_2}{\Gamma} + 1\right)\frac{2}{\delta^2}$, $\nu = 4g\left(1 - \frac{2}{\gamma}\right)$ and $g = \frac{M_2}{4\delta^2} \sim N^2/16$. Now one may rewrite everything in a scale-free way in terms of a single parameter, 'a':

$$\left[-\frac{d^2}{dz^2} + a z^2 + z^4\right]\phi_n = \epsilon_n(a)\phi_n\,, \tag{10}$$

with scale-free coordinates $z = y g^{1/6}$, $\psi(y) = g^{1/12}\phi(z)$, $a = \nu/g^{2/3} = 4g^{1/3}(1-2/\gamma)$ and $\epsilon_n = \tilde{E}_n/g^{1/3}$. At the critical point $\nu = a = 0$, and the eigenvalue problem is reduced to that of the pure quartic potential. Note that the energy spectrum, including ϵ_0, and the half-width of its ground-state, let's call it z_0, are pure numerical values. Scaling back from ϵ_n to E_n indicates that the spectrum is compressed near the critical point,

$$\Delta E_{k\ell} = \frac{\Gamma \Delta\epsilon_{k\ell}}{2(4^{1/3})j^{4/3}} \qquad (\Gamma \approx 2/3)\,. \tag{11}$$

Remembering that $\Delta\epsilon_{k\ell} = |\epsilon_k - \epsilon_\ell|$ is a pure number, the energy gap in the original problem is compressed by $j^{-1/3}$ compared with the strong or very weak transverse field Regions I and III, where it is uniform in $j\hat{H}$, as we shall see in section VI. The compression of eigenvalues can be inspected in FIG.2 for an $N = 100$ ensemble. Establishing the true length-scale for y involves dividing $z_0/g^{1/6} \propto \delta^{1/3}$ or $j^{-1/3}$, without having to recover any features of the wavefunction explicitly. Recall that $y = m/j$; the width scales as $j^{2/3}$ in m, or indeed $N^{2/3}$. As we hoped, this partially-entangled 'Goldilocks' state at the critical point has greater width than the Gaussian separable distribution of width $\sqrt{N}$ associated with a spin-coherent state (such as the ground state at $\Gamma = 1$).

V. LOCATION OF MINIMUM GAP

From the beginning, our desire has been to prepare a Goldilocks probe via quantum annealing – we reduce the transverse field adiabatically, keeping the system in the instantaneous ground state at all times. The annealing must proceed especially slowly when the gap between ground and excited states is smallest, avoiding diabatic passage into another eigenstate whose contribution to precision may be negative. It is necessary, therefore, to establish the size and location of the minimum gap during the schedule, as this will be the dominant bottleneck affecting efficient probe preparation.

Close to the critical point in the thermodynamic limit, $|a| \ll 1$. In the scale-free setting, one could potentially treat the $\langle z^2\rangle$ term of eqn. (10) perturbatively, $\epsilon_0(a) = \epsilon_0(0) + a\epsilon_0'(0) + \ldots$.It turns out, however, from an exact numerical analysis shown in FIG.2 (b) and FIG.3 (b), that the minimum gap $\epsilon_2(a_0) - \epsilon_0(a_0)$ does not correspond to a convergent perturbative regime, since $|a_0| > 1$. We focus on the $0 \leftrightarrow 2$ energy level transitions because there is no matrix element between the ground and first excited states; they have opposite parity.

The annealing parameter Γ_0 at the minimum gap may be identified as:

$$\Gamma_0 = \frac{\Gamma_c}{1 - \frac{a_0}{12 g^{1/3}}} \approx \Gamma_c + \left(\frac{4^{1/3}a_0}{18}\right)\frac{1}{j^{2/3}} + \left(\frac{2^{1/3}a_0^2}{108}\right)\frac{1}{j^{4/3}}\,, \tag{12}$$

again recalling the relation $a = 12g^{1/3}(1 - \Gamma_c/\Gamma)$, and substituting $a \mapsto a_0$ and $\Gamma \mapsto \Gamma_0$. Using the numerical result $a_0 \approx -3.9556$, the prefactor to the dominant $j^{-2/3}$ scaling of $\Delta\Gamma_c = \Gamma_c - \Gamma_0$ is approximately 0.349. Prefactors and scaling for the leading terms are confirmed by comparison with the minimum gap of the original spin problem for different ensemble sizes j in FIG.3 (c). Throughout this paper our goal is to map out this spin system's features in the Goldilocks critical region at finite ensemble size N, including the dominant 'finite-size effects'. The apparent discontinuities occurring in the thermodynamic limit $N \sim \infty$ provides no guidance here, as the Goldilocks zone vanishes in this limit.

From the shape of the ground-state wavefunction ϕ_0, the red curve plotted in FIG.3 (a), it is apparent that modelling the ensemble approximately as a large coherent spin state, as is done in classical mean-field models, is not valid near the minimum gap; the distribution is clearly not even unimodal here. Neither is it accurate to model the state as a GHZ-like bimodal distribution, as in Region I. A more faithful description, as we have seen, is a ground state of a *quartic* potential.

VI. GROUND STATES: REGIONS I AND III

Ref.9 proposed annealing all the way from a spin-coherent state in Region III to a 'Schrödinger Cat' (GHZ/NOON-like) state in Region I. A similar technique was advocated in Ref.29 where atom-atom couplings were generated via interaction with a strong classical driving field in a thermal cavity to produce multi-atom states such as the GHZ state. At $\Gamma = 0$ the

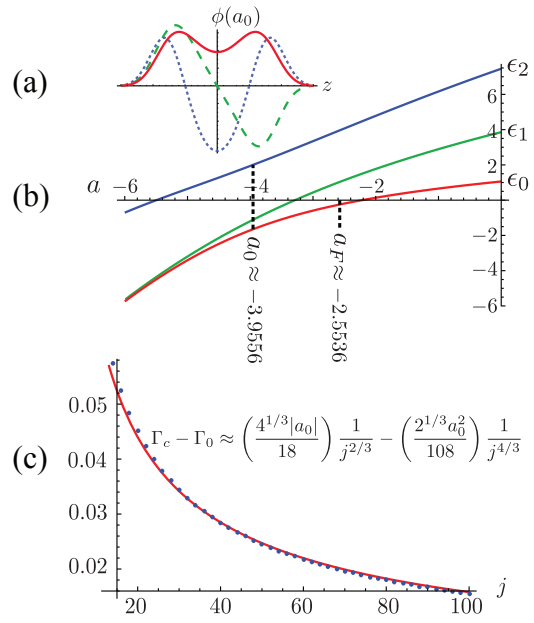

FIG. 3: Rescaled Spectrum: the eigenstates $\phi_{0,1,2}$ (unbroken, dashed, dotted lines) in (a) and energy eigenvalues $\epsilon_{0,1,2}$ in (b) found numerically for the scale-free quartic potential from eqn. (10) with single parameter a. The minimum gap a_0 and maximum precision point a_F are indicated. In the third sub-plot (c), blue points show the difference $\Delta\Gamma$ between the value of the annealing parameter at the minimum gap Γ_0 and the $j \gg 1$ critical point $\Gamma_c = 2/3$ in the original discrete spin Hamiltonian of eqn.(1). The (red) unbroken curve in subplot (c) has function $0.349/j^{2/3} - 0.183/j^{4/3}$ derived in section V.

ground state is exactly a GHZ state and, as the field is ramped back up, its two delta components broaden into symmetrized ($|\psi_+\rangle + |\psi_-\rangle$) or anti-symmetrized ($|\psi_+\rangle - |\psi_-\rangle$) pairs of Gaussian lobes, FIG.1. Close to the well bottoms $\pm y_0$ the potential is predominantly quadratic. One must remember that this is a position-dependent mass problem and that the mass function is well-approximated by its value at y_0. $M(y_0) = M_\gamma + O(\delta^2)$ for $\gamma < 2$, where $M_\gamma = 2/\gamma$. The mass increases monotonically with decreasing transverse field. To second order $V(y) = V_0 + V_0''(y \pm y_0)^2/2$ close to turning points $\pm y_0 = \pm\sqrt{1 - M_\gamma^{-2}} + O(\delta)$, where $V_0 = -(M_\gamma + M_\gamma^{-1})/2$ and $V_0'' = M_\gamma(M_\gamma^2 - 1)$.

Overall we have a superposition of twin harmonic oscillators with frequency $\omega = \sqrt{M_\gamma^2 - 1}$, minimum gap $E_2 - E_0 = \delta\omega$ and ground state energy $E_1 \approx E_0 = \delta\omega/2$, indicating the almost degeneracy between the even and odd parity eigenstates, $|\psi_+\rangle \pm |\psi_-\rangle$.

This approximation at quadratic turning points has been shown robust, even outside the wells extending into much of the forbidden central barrier region [26]. The width $\sigma = \sqrt{\delta/(M_\gamma\omega)}$ of each Gaussian lobe in the y variable increases monotonically with the applied field and one may write $\sigma = \Sigma/\sqrt{N}$ where coefficient Σ is independent of N. The small tunneling probability through the barrier slightly lifts the energy of the anti-symmetric state $|\psi_+\rangle - |\psi_-\rangle$, but this gap remains exponentially small in N. The energy gap to the second and third excited states, also nearly degenerate, is approximately $\delta\omega$. (In fact, the Sturm-Liouville theorem guarantees that there can be *no* degeneracies in a one-dimensional system, and that pairs of almost degenerate states are grouped with odd states above the even states – see for instance Ref.30.)

In the strong transverse field of Region III, the pseudo-potential $V(y)$ of eqn.(8) is dominated by its quadratic term, $V(y) \approx -1 + (1 - 2/\gamma)y^2/2$ and the eigenstates will be approximately those of a harmonic oscillator centered on $y = 0$; therefore the effective mass remains $M_2 \approx 1$, and is no longer a function of the applied field for $\gamma > 2$. The Schrodinger equation for the strong transverse field is:

$$\left[-\frac{\delta^2}{2M_2}\frac{d^2}{dy^2} + \frac{M_2}{2}\left(1 - \frac{2}{\gamma}\right)y^2\right]\psi_n = \left(\frac{E_n}{\Gamma} + \frac{1}{M_2}\right)\psi_n \tag{13}$$

The unnormalized eigenstate is $\langle y|\psi_0\rangle \propto \exp\{-jM_2(\sqrt{1 - 2/\gamma})y^2/2\}$. Collecting these results, in the thermodynamic limit ($N \gg 1$) the energy gap of $j\hat{H}$ is

$$\omega = \sqrt{(\Gamma - 2)(3\Gamma - 2)}\,, \qquad (\Gamma < \Gamma_c) \tag{14a}$$

$$= 2\Gamma\sqrt{3 - 2/\Gamma}\,, \qquad (\Gamma > \Gamma_c)\,. \tag{14b}$$

We shall see in subsequent sections how these three qualitatively very different ground states: the bimodal distribution in Region I; the broad centrally-weighted Goldilocks state in Region II; and the Gaussian state in Region III, compare as interferometric probes. In the appendix, we also examine the entanglement present during the annealing through the three regions.

VII. QUANTUM PARAMETER ESTIMATION IN PRESENCE OF NOISE

It would seem that the Goldilocks state in Region II has some of the right qualitative features for metrology. To quantify the supra-classical precision in e.g. estimation of an interferometric phase θ, the mean-squared error $\Delta^2\theta$ is lower-bounded by the Cramer-Rao inequality,

$$\Delta^2\theta \geq 1/(kF)\,, \tag{15}$$

where k is the number of repetitions of the experiment and F is the quantum Fisher information (QFI). Our objective in quantum metrology is usually to maximize this objective function F, which depends on both probe state $|\psi\rangle$ and the dynamics during phase acquisition. The formalism developed in Refs. 7, 31 for realistic noise processes (incorporating dephasing, relaxation, excitation) presents the QFI as an exact asymptotic series in powers of $1/j$ or $1/N$. Writing $d\psi/dy$ as $\psi'(y)$ the QFI for estimation of a phase θ associated with unitary evolution under $\hat{J}_z$ in the presence of 'real-world' noise

has the form of a generalized 'action':

$$\frac{F}{N^2} \simeq \int_{y=-1}^{+1} \frac{\psi(y)^2}{\mu(y)} dy \; - \; 4 \int_{y=-1}^{+1} \frac{\psi'(y)^2}{\mu^2(y)} dy \; , \qquad (16)$$

excluding cubic and higher powers of $1/\mu(y)$, as is valid in the $N \gg 1$ asymptotic limit. Above in the action integral, the 'noise function' $\mu(y) > 0$ produces an effective mass in the kinetic term and $1/\mu(y)$ plays the role of a potential. This function μ is proportional to N or N^2, depending on the type and strength of the noise present, see appendix D.

From eqn. (16), it is apparent that, for large ensembles $N \gg 1$, only those state profiles $\psi(y)$ with smoothly-varying features will be optimal. The term squared in the gradients $\psi'(y)$ has a negative sign, penalizing QFI, and therefore precision. Optimal interferometric probes should have real amplitudes in the $\hat{J}_z$ or y basis, at least for the quite general types of noise we will examine, because robustness to noise depends on the survival of off-diagonal amplitudes. If these real (not complex) noise processes mix state amplitudes into off-diagonal matrix elements, those elements will have greater size if the component amplitudes are all real. (A mixture of amplitudes with different phases will have smaller overall amplitude.)

VIII. INTERFEROMETRIC PERFORMANCE OF GOLDILOCKS GROUND STATE

Consider a combination of classical phase fluctuations of size $\Delta\theta = \sqrt{\kappa^0}$ and local noise $\kappa^{(L)}$. Putting $\mu(y) = N^2\kappa^0 + N\kappa^{(L)}/(1-y^2)$ (more details in the appendix) into eqn.(16) means calculating terms like the second moment $\langle y^2 \rangle = \int_y y^2 \psi^2(y)(dy)$, and paying particular attention to the *penalty* terms featuring squared gradients: $\int_y \psi'(y)^2 (dy) = \delta^{-2} \langle \hat{P}^2 \rangle$, (because $\psi'(y) = i\delta^{-1}\hat{P}\psi$). We might naively propose the 'phase' state, which has $\psi_m = 1/\sqrt{N+1}$ for $m \in [-j, +j]$ as a quantum probe; it is a completely flat distribution. But it produces a large spurious gradient $\propto \sqrt{N}$ at the boundary between $\psi_j = 1/\sqrt{N+1}$ and $\psi_{j+1} = 0$ remembering the definition of eqn. (4a). Also, the role of the probe component variance, or equivalently, the amount of 'squeezing' is significant; it is not simply that more is better. Optimal probes will have variance dictated by the strength of noise present.

For a Goldilocks state close to the critical point $\gamma_c = 2$, let us examine the dominant penalty term, $\delta^{-2}\langle \hat{P}^2 \rangle$. For eigenstates of H it is easy to show $\langle [\hat{H}, \hat{P} y] \rangle = 0$ and calculating this commutator[57] provides an expression for $\langle \hat{P}^2 \rangle$. Expanding to y^4 near $y = 0$ and converting to the scale-free variable z gives:

$$\begin{aligned} \frac{\langle \hat{P}^2 \rangle}{\delta^2} &= 4 \left(1 - \frac{2}{\gamma}\right) g^{2/3} \langle z^2 \rangle + 2 g^{1/3} \langle z^4 \rangle \\ &= g^{1/3} \left(a \langle z^2 \rangle + 2 \langle z^4 \rangle \right) \end{aligned} \qquad (17)$$

But we also have, from the Schrödinger equation, that $\langle \hat{P}^2 \rangle / \delta^2 = g^{1/3} [\epsilon_n(a) - a\langle z^2 \rangle - \langle z^4 \rangle]$ so we can eliminate

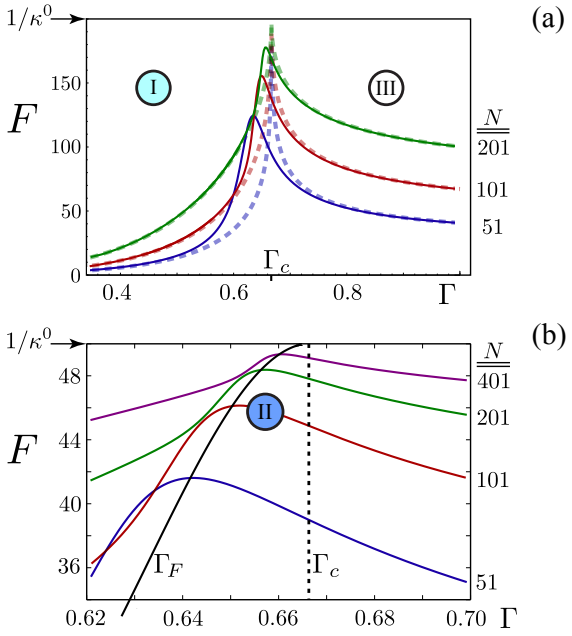

FIG. 4: Numerics and analytics compared for collective dephasing: In (a), dashed curves show precision $F(\Gamma) \leq 1/\kappa^0$ for analytic ground states of Regions I and III in the thermodynamic limit; states discussed in section VI and precision given in eqn.(23). Here $N = 51, 101, 201$ qubit ensembles are subjected to collective dephasing $\kappa^0 = 1/200$. Exact numerical results are unbroken curves of the same colour, with the calculation proceeding as follows. First, ground states of the original spin problem are found by direct matrix diagonalization. Second, the QFI is calculated by additional diagonalization of the mixed state to which the ground state evolves under decoherence, see eqn. (C1) in the appendix. The discrepancy between dashed/unbroken curves in the upper figure (a) is due to the absence of (Goldilocks) Region II in the thermodynamic limit (dashed curves). The lower plot (b) zooms in on the critical region for larger dephasing $\kappa^0 = 1/50$ and $N \in \{51, 101, 201, 401\}$. Coloured curves are still numerical results of QFI. The steep unbroken black curve in (b) gives the analytic locus of the predicted QFI maxima $\{\Gamma_F, F(\Gamma_F)\}$ for all finite N, using the asymptotic results of eqns. (19) and (20). The formula for $F(\Gamma_F)$ is only valid when the condition $\kappa^0 N^2 \gg 1$ is met, as it is in (b).

$\langle z^4 \rangle \mapsto (\epsilon_n(a) - 2\langle z^2 \rangle)/3$. Identifying $\epsilon'(a) = d\epsilon(a)/da = \langle z^2 \rangle$ using the Hellmann-Feynman theorem for parameter a gives the precision penalty factor (PPF):

$$\frac{\langle \hat{P}^2 \rangle}{\delta^2} = \frac{g^{1/3}}{3} \Big(2\epsilon_0(a) - a\epsilon_0'(a) \Big) \; . \qquad (18)$$

An exact numerical search (finding the zero point energy in the quartic potential as a function of a) reveals $a \mapsto a_F \approx -2.5536$. This parameter value a_F minimizes the PPF above at $1.4239 g^{1/3}/3$; this is analogous to how the location a_0 of the minimum gap was found earlier, see plot (b) of FIG. 2. Scaled back to the annealing variable Γ, optimal precision oc-

curs at:

$$\Gamma_F = \Gamma_c \left(1 - \frac{a_F}{12 g^{1/3}}\right)^{-1} = \Gamma_c \left(1 - \frac{a_F}{3}\left(\frac{1}{2M_2 N}\right)^{2/3}\right)^{-1} \tag{19}$$

Note that this optimum point on the annealing schedule is not a function of the decoherence strength or type – it depends only on the number of qubits (to leading order).

The expansion of minimum error is:

$$\left[\Delta^2\theta\right]_{\rm II} \geq \frac{1}{F(\Gamma_F)} = \kappa^0 + \frac{\kappa^{(L)}}{N} + \frac{2}{3N^{4/3}}\left(\frac{M_2}{2}\right)^{\frac{1}{3}}\left(2\epsilon_0(a_F) - a_F\epsilon_0'(a_F)\right) \tag{20}$$

ignoring terms $O\left(1/N^{5/3}\right)$ and smaller. The leading two terms are independent phase errors from collective phase noise and local noise that has shot-noise scaling $\propto 1/N$. Together, they represent the lowest possible mean squared phase error. The next significant term, in $1/N^{4/3}$, would provide the leading N dependence in the absence of local noise. It also dictates how fast the bound $\kappa^0 + \frac{\kappa^{(L)}}{N}$ may be approached in an asymptotic sense (the more negative is the power of N in the third term above, the faster the convergence). Note that both κ^0 and $\kappa^{(L)}$ are absent from this term $\propto N^{-4/3}$, its contribution to phase error comes from $\langle \hat{P}^2 \rangle$ alone, i.e. the probe shape. The generic $1/N$ scaling of precision for most quantum channels was first derived in Ref.(32) and later, optimal probe shapes were found for lossy interferometry [33].

It should be emphasized that this result, eqn. (20), is generic for any combination of local and collective noise (parameters κ^0 and $\kappa^{(L)}$) including noise that is completely one or the other. The differing functional dependence of $\mu(y)$ in each case plays a sub-leading role, arising at the $O\left(1/N^{5/3}\right)$ level or smaller. FIG.5 shows the precision curves $F(\Gamma)$ for different types of noise of equivalent strength.

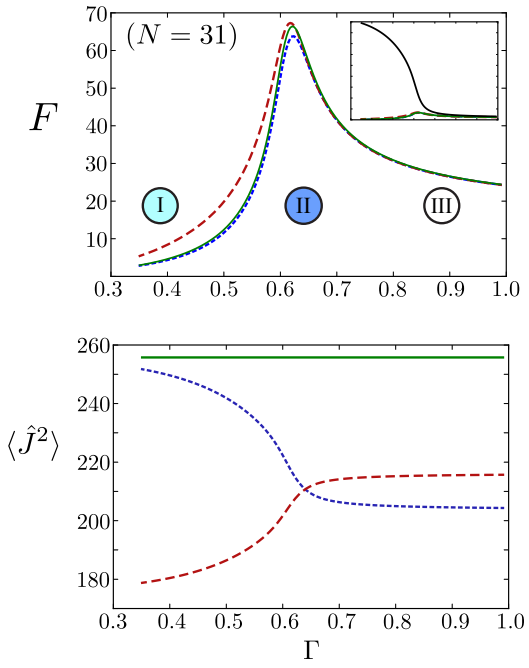

FIG. 5: Local vs. Global Noise: For $N = 31$ qubits, processes of collective/global/correlated dephasing (green continuous curve), individual/local/uncorrelated dephasing (blue dotted curve) and local relaxation (red dashed curve) are seen to have the same detrimental effect on precision F for the annealed system. To leading order they all produce the same characteristic precision curve (upper plot) for the full range of values of the annealing parameter Γ. The inset plot shows the performance in the noiseless case (unbroken black line) compared with the three noisy scenarios, which it dwarves in Region I (it approaches $F = N^2$ at $\Gamma = 0$). When instead the expectation value of the spin operator $\hat{J}^2$ is plotted (lower plot) one observes that collective dephasing preserves the overall spin quantum number $j = j_{\rm max} = 31/2$, so $j(j+1) = (31/2) * (33/2)$. Local noise, in contrast, results in drift and diffusion of the probe state into lower spin spaces. Local relaxation (red/dashed line) of the GHZ-like state in Region I is particularly symmetry-breaking, resulting in a substantial drift into lower spin spaces. All three noise processes, however, dramatically reduce the precision of this fragile superposition state; F approaches zero for all decoherence types in the weak field limit, $\Gamma \sim 0$. We chose $\{\kappa^0, \kappa^{(L)}\} \mapsto \{0.009, 0\}$ for collective dephasing and $\{0, 31 * 0.009\}$ for local noise, deliberately keeping the overall precision limit the same: $F < 1/(\kappa^0 + \kappa^{(L)}/N)$ and to illustrate how similar the F curves can be. Appendix D has more detailed discussion of noise. For the local nosie case the qubits are each coupled to their own individual bosonic baths, rather than to the same bath, as in the collective noise case.

IX. INTERFEROMETRIC PERFORMANCE OF GROUND STATE IN STRONG AND WEAK FIELDS

To contrast, for increasing transverse field $\Gamma > 2/3$ the ground-state is an approximately Gaussian-distributed wavefunction $\psi(y) \propto \exp\{-jM_2(\sqrt{1-2/\gamma})y^2/2\}$, becoming eventually a spin-coherent state aligned with the field in the spatial x-direction, a separable state. For $1/F$ one recovers an exact expression bounding the mean squared phase error:

$$\left[\Delta^2\theta\right]_{\rm III} \geq \kappa^0 + \left(M_2\sqrt{3-2/\Gamma} + \kappa^{(L)}\right)/N\ . \tag{21}$$

It appears that the ultimate lower bound $\kappa^0 + \kappa^{(L)}/N$ can be approached in the limit $\Gamma \sim 2/3$; the associated Gaussian wavepacket would, however, have infinite variance. But for $\kappa^{(L)} < 1$ and smaller $\kappa^0 < \kappa^{(L)}/N$, there exists a good argument for preparing the probe state as close to Γ_c as possible. The error minimum predicted above for Region III at criticality, combined with the more accurate results derived previously for Region II, both promote the vicinity of Γ_c as optimal for probe preparation. But what about Region I?

In Region I, transitions between the ground state $|\psi_+\rangle + |\psi_-\rangle$ and first excited state $|\psi_+\rangle - |\psi_-\rangle$ are prohibited, due to their opposite parity and because evolution via the time-dependent Schrödinger equation is parity-conserving. Unfortunately, any noise or decoherence is *unlikely* to respect parity, so even at very low temperatures, thermalization occurs to an equal mixture of the two near-degenerate states. Such

an effectively 2-level (qubit) maximally-mixed state will be symmetric under unitary evolution by the interferometric $\hat{J}_z$ operator, and useless in estimating the phase parameter[34].

Let us imagine that the symmetrized superposition of gaussians *could* be prepared adiabatically. For hybrid noise, the QFI 'action' integral of eqn.(16) produces:

$$\left[\Delta^2\theta\right]_{\rm I} \geq \kappa^0 + \frac{1}{N}\left\{\kappa^{(L)}(1+y_0^2) + \frac{1}{\Sigma^2}\right\} + O\left(\frac{1}{N^2}\right)$$
$$= \kappa^0 + \frac{1}{N}\left\{\kappa^{(L)}\left(2 - \frac{1}{M_\gamma^2}\right) + M_\gamma\sqrt{M_\gamma^2 - 1}\right\} + O\left(\frac{1}{N^2}\right) \quad (22)$$

approximately valid as long as the wells retain a parabolic shape across the width of the ground-state lobes. Notice that, for this noisy scenario, error increases with the width of the central barrier separating the two wells $2y_0$ (shown in FIG.1) and there is a additional precision penalty for narrower Gaussian lobes of width $\sigma = \Sigma/\sqrt{N}$; the opposite behaviour is seen in a noiseless environment, where QFI increases quadratically with the ratio y_0/σ. Apparently, wider lobes that are closer together (less 'cat-like') improve robustness to noise.

In the limit $\Gamma \sim 0$, the assumption of smoothly varying ground state amplitudes is no longer valid– the state is in reality a NOON or GHZ state, whose interferometric performance in the presence of noise has been shown elsewhere to scale exponentially badly in ensemble size N. For collective dephasing QFI is $N^2\exp\{-\kappa^0 N^2\}$ and in dissipative systems of transmission $\eta < 1$ it is $\mathrm{N}^2\eta^N$. (Refs.35, 36).

The unbroken curves in FIG.4 show the performance $F(\Gamma)$ calculated numerically for the original spin system in the presence of interferometric phase noise. These curves asymptote for $N \gg 1$ to give the analytical result in the thermodynamic limit :

$$F_\infty(\omega) = \left(\kappa^0 + \frac{\kappa^{(L)}}{N} + \frac{M\omega}{N}\right)^{-1}, \quad (23)$$

where ω is given in eqn.(14) and $M \mapsto M_\gamma = 2/\gamma$ for $\gamma < \gamma_c$ and $M \mapsto M_2 \approx 1$ for $\gamma > \gamma_c$. The asymptotes ignore the critical region entirely; recall that it vanishes in $\Delta\Gamma$ near Γ_c at a rate $\propto 1/N^{2/3}$.

Comparing $1/F_\infty(\omega)$ with eqn.(20) we see explicitly that the ultimate precision limit $\kappa^0 + \kappa^{(L)}/N$ is *only* asymptotically saturable in Region II; in the other regions there is an additional contribution to mean squared error of order $1/N$ proportional to the gap ω. This is a central result of this paper.

X. ANNEALING TIME COMPLEXITY

Annealing time can depend on the requirement of adiabaticity – whether the system needs to be in the instantaneous ground state at all times. If this can be relaxed, the annealing time can be reduced. Roughly speaking, the annealing schedule must progress slowly when the gap between the ground and first excited state is small. The exponential scaling in N of the time complexity of certain quantum algorithms can be traced to an exponentially small minimum gap. In the current context, the gaps for $j\hat{H}$ in Regions I and III are fixed and independent of j or N (derived from the ground state approximation calculated in section VI). That leaves only Region II. Choosing the final annealing parameter as Γ_τ and using a prescription from Ref. 37, an optimal annealing time T can be calculated as

$$T \approx \int_{\Gamma_\tau}^{1} \left|\left|\frac{d(j\hat{H})}{d\Gamma}\right|\right|_2 \frac{d\Gamma}{\omega^2(\Gamma)}, \quad (24)$$

where $||M||_2$ is the 2-norm of a matrix M. For the current Hamiltonian $\left|\left|\frac{d(j\hat{H})}{d\Gamma}\right|\right|_2 = \left|\left|\hat{J}_z^2/j - \hat{J}_x\right|\right|_2 \sim 5j/4$ for $j \gg 1$. This matrix norm factor is linear in N and independent of Γ throughout all regions. As presented in eqns. (14), irrespective of where the annealing is halted the contributions from $1/\omega^2$ in both Regions I and III approaches a constant, leaving only the calculation for Region II. There, $\Gamma_\tau \subset \Gamma_c \pm \Delta\Gamma_G$, and the gap $\omega_{\rm II} = \Delta E_{20} \propto j^{2/3}/\Gamma$ from

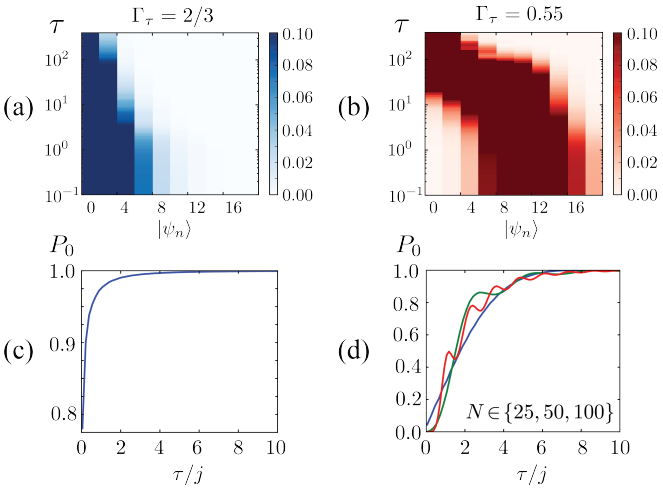

FIG. 6: Annealing: Upper plots (a) and (b) show for $N = 100$ the overlap $|\langle\psi|\psi_n\rangle|$of the annealed state with the 20 lowest energy states $|\psi_n\rangle$ with $n \in \{0, 19\}$ subject to a linear annealing schedule of total time τ, so $\Gamma(t) = 1 - (1-\Gamma_\tau)t/\tau$. Odd-numbered energy eigenstates are excluded because their overlap with the annealed state is zero at all times. They have odd parity and the annealing Hamiltonian respects the even parity of the initial state at $t = 0$. On the left, the annealing schedule is terminated at the critical point $\Gamma_\tau = \Gamma_c$, and on the right, it is terminated some way into Region I after traversing the minimum gap. When the annealing is halted in the critical region, the instantaneous ground state is still dominant across many orders of annealing time. The lower two plots (c) and (d) show the probability P_0 to be in the target ground state, again for an annealing cycle halted at $\Gamma = 2/3$ and 0.55. The horizontal axis is the total annealing time in the linear schedule, in units scaled by the number of qubits: τ/N. The blue, green and red curves are for systems of 25, 50 and 100 qubits, respectively; larger systems exhibit more fluctuations about the same general trend in (d). In (c), the three trend curves are identical and smooth, exhibiting no superimposed fluctuations. Annealing success for a linear schedule apparently scales linearly with ensemble size, discussed in section X.

eqn. (11). Then we have an annealing time $T_{\rm II} \approx$

$$\frac{5j}{4}\int_{\Gamma_c-\Delta\Gamma_G}^{\Gamma_c+\Delta\Gamma_G}\frac{d\Gamma}{\omega_{\rm II}^2(\Gamma)} \propto j^{\frac{5}{3}}\int_{\Gamma_c-\Delta\Gamma_G}^{\Gamma_c+\Delta\Gamma_G}\frac{d\Gamma}{\Gamma^2} \sim j^{\frac{5}{3}}\frac{\Delta\Gamma_G}{\Gamma_c^2} \propto j \tag{25}$$

where, in the last step, we have recalled that the Goldilocks zone scales $\Delta\Gamma_G \sim j^{-2/3}$.

Overall time complexity is $T \sim O(j)$ in all three annealing regions. This estimate could be considered pessimistic as it applies only to adiabatic passage. For a linear annealing schedule, numerical results confirm that, irrespective of where the annealing is halted (near criticality or all the way to the weak field limit), the annealing time for any desired fidelity to the target ground state is linear in N, see FIG.6. Whether terminating at a GHZ-like state or Goldilocks probe, the total time differs only by a fixed factor independent of N. Since the annealing time scales favorably with the size of the ensemble, then decoherence may be less significant during probe preparation.

XI. CONVERGENCE ON ASYMPTOTICS

In the scale-free setting of Region II, the pure numerical values of minimum gap and precision penalty factor are predicted to be $\epsilon_2(a_0)-\epsilon_0(a_0)$ and $2\epsilon_0(a_F)-a_F\epsilon_0'(a_F)$, respectively. This latter minimum corresponds to maximum QFI. If instead the maximum QFI is found by brute force numerical diagonalization and eqn.(C1) for different ensemble sizes N and collective phase noise amplitude κ^0, the true penalty factor can be determined including all finite-size corrections. The ground-state gap in the original spin dynamics ΔE_{20} is also easily converted into that of the scale-free setting. The convergence to the predicted asymptotic values is seen in FIG.7. From these graphs it is clear that convergence is fairly slow, but by $N \approx 10^3$ and $\mu_0 > 10^4$ the numerical values do approach these asymptotic bounds. This observation provides crucial evidence in validating the sequence of approximations that have been made; mapping from a spin system to a 1-D particle in a potential, restriction to a quartic potential in the critical region, and approximation of the QFI by its two leading terms in the exact asymptotic series. The reason for the slow convergence could be attributed to the first term excluded from the QFI series being only slightly smaller than the last included term, $N^{-5/3}$ vs $N^{-4/3}$. The value of N has to become quite large before $N^{-4/3}$ can dominate.

XII. CONCLUSIONS AND OUTLOOK

We have examined a network of uniformly-coupled spins in a transverse field as an interferometric probe for use in noisy conditions. Mapping the ensemble onto a variable-mass particle in a potential allowed quantitative understanding of the dynamics in the critical region, i.e. we were able to characterize correctly the dominant properties of the continuous phase transition. In terms of annealing parameter Γ, we discovered

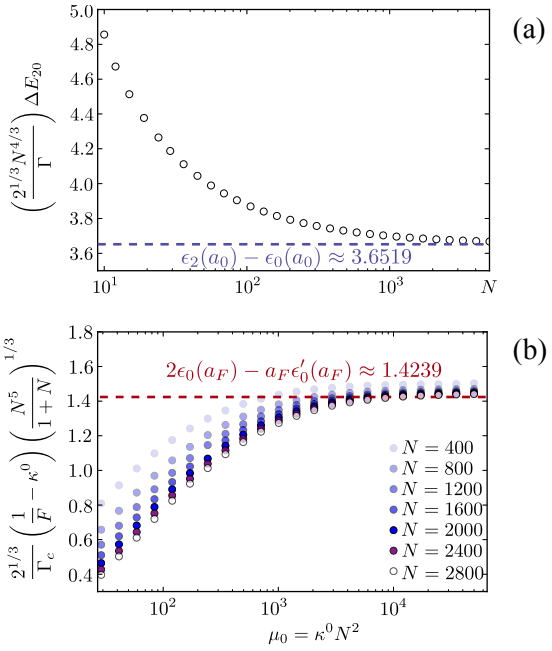

FIG. 7: Convergence to Asymptotics: Vertical axes plot pure numerical factors expected to converge on $\epsilon_2(a_0)-\epsilon_0(a_0)$ in (a) and $2\epsilon_0(a_F)-a_F\epsilon_0'(a_F)$ in (b), a re-arrangement of eqn. (11) and eqn.(20). The asymptotic predictions are 3.6519 and 1.4239, respectively for the gap and penalty factor (blue and red dashed lines). Since these derive from the scale-free picture, they are independent of both Γ and N.

the ordering and distances between the critical point in the thermodynamic limit Γ_c, the minimum gap Γ_0 and the point of maximum precision Γ_F using an exact numerical approach. These latter landmarks are the relevant ones for annealing and metrology, and are sufficiently far from Γ_c that conventional perturbative techniques would fail. Utilizing asymptotic formulae for QFI, we predicted that in a noisy environment, best precision is offered *only* by ground states prepared near the critical point. We saw in eqn.(20) that such states asymptotically *saturate* the ultimate precision bounds for interferometers subjected to typical noisy environments. We confirmed the accuracy of both the asymptotic QFI expansion and the legitimacy of the continuous particle mapping by brute force matrix diagonalization methods for the original spin system, for $N \in [30, 3000]$. (In the asymptotic approach, only the combined parameter μ is required to be large – the product of noise strength and ensemble size.) We determined that adiabatic probe preparation has a time-complexity scaling linearly with ensemble size.

In Ref. 7 the calculus of variations dictated that asymptotically the best-performing interferometric state was *always* the ground state of a 1D particle in a special pseudo-potential, created between two repulsive Coulomb sources and identical to the noise function $\mu(y)$. In some sense, we have tried to engineer non-linear dynamics that best mimic that optimal potential. Although a quartic potential does not much resemble the optimal one, any ground state of width in the variable

y that narrows with increasing N will not 'explore' the structure of the potential far from $y = 0$; such a probe can have some of the desired properties in the large N limit.

Decoherence during probe preparation must be strongly suppressed, e.g. fluctuations in the transverse field γ are amplified in the a variable[58] by $N^{2/3}$ – the strength of these fluctuations places an upper limit on the size of the spin ensemble that can be prepared in the critical region. The full effects of decoherence during the annealing schedule we leave to a future publication. Certainly, thermal transitions between $\epsilon_0 \leftrightarrow \epsilon_1$ will always be problematic throughout the annealing schedule – at least to the critical point this gap is polynomially rather than exponentially small. Because the energy eigenbasis is constantly rotating during annealing, one must also consider that Kraus jump operators physically responsible for excitation and relaxation at the beginning of the schedule may play the role of dephasing or some other combined process inside the critical region.

The results of this paper promote an alternative perspective on the developing technology that is the quantum annealing machine, e.g. the pioneering work of Ref.40. Typically, the goal of such devices is to prepare a ground state that represents the optimal solution to a combinatorial problem encoded directly in the couplings of an Ising Hamiltonian. Here, it has been proposed that such customizable dynamics might instead be used to prepare some exotic, yet useful, multi-qubit quantum state. Perhaps the application is metrology as discussed; other possibilities include quantum communication, or generation of different types of entanglement[41] for distributed quantum information. Presented in the context of ion traps and optical lattices, the authors of Ref. 42 had already recognized the potential of a Dicke-Ising model of quantum computing for simulation of quantum systems, and as a resource for generating squeezing and entanglement. More recently, the creation of tunable Ising systems optically has been proposed in QED cavities[43] but not yet considered for metrology applications.

The inverted challenge in terms of global optimization is to 'reverse engineer' the Ising couplings to prepare a particular known ground state of interest. Now, the search objective is the associated Hamiltonian couplings and topology. When preparation time is a significant resource, one may have to offset state fidelity against shorter annealing times, if the landscape necessitates annealing through gap regions, or if adiabaticity is not a strict requirement. Adding external control fields might avoid proximity to the smallest gaps, and allow adiabatic short cuts[44] such as transitionless driving[45].

XIII. ENDNOTE

A final sidelight to our proposal is provided by an earlier scheme[46], due originally to Kitagawa and Ulam-Orgikh, that uses entangled quantum spin states for noisy frequency estimation. (It was analyzed recently and more comprehensively in terms of Fisher information in Ref.47.) Beginning with the same spin-coherent state aligned with the strong transverse field, subsequently the field is *abruptly* and discontinuously stepped to zero. The ensemble then evolves diabatically for some time under the influence of its $\sigma_z^{(1)}\sigma_z^{(2)}$ couplings. After a particular elapsed time t, the state is rotated by an angle θ around $\hat{J}_y$ to produce an optimal probe for noisy interferometry. The propagator is effectively $\exp\{-i\hat{J}_y\theta\}\exp\{-i\hat{J}_z^2 t/j\}$ acting on the spin coherent state. In such proposals, for ν repeated independent trials with a single instrument, the overall time $T = \nu t$ is considered a resource and kept constant, whereas the individual interrogation time t is optimized over. Typically an optimal t is found to be very small; the amount of necessary squeezing is very slight, as is the effect of decoherence. These proposals are examined in depth in the encyclopedic work on spin squeezing by Ma, Wang, Sun and Nori [48].

One might now ask whether it is more feasible to prepare optimal probes by manipulating two control parameters diabatically, or just a single parameter, under the constraint that it be attenuated adiabatically. For both adiabatic and diabatic schemes the 'sweet-spot' of supra-classical performance in parameter space (Γ, or t and θ) shrinks dramatically with increasing N – experimentally it becomes a challenge to reach. It is not clear yet which approach is more amenable to experimental implementation as our proposal has not been considered previously. In terms of feasibility, prior work on frequency estimation allowed for instantaneous resetting of the instrument/interferometer (zero dead-time) and arbitrarily short interrogation times t, which may be outside the realm of possibility for real instruments and detectors, and may violate Markovian principles. (In a sequence of independent interrogations of the phase, the instrument and environment must have no memory of the previous evolution and measurement; one therefore cannot neglect, for example, the auto-correlation time of the environment/bath. The limit $t \sim 0$ is thus forbidden.) Certainly a direct comparison of the adiabatic and the diabatic squeezing approaches for probe preparation and phase estimation under realistic local and global noise should be the subject of future work.

Acknowledgements

During the course of this study I had several useful discussions with Zhang Jiang and Sergey I. Knysh at NASA Ames Research Center, and Itay Hen at the Information Science Institute of the University of Southern California. Assistance with literature review was provided by algorithms developed by the team at lateral.io

[1] Demkowicz-Dobrzański, R., Jarzyna, M. & Kołodyński, J. Quantum limits in optical interferometry. *Progress in Optics* (2015).

[2] Giovannetti, V., Lloyd, S. & Maccone, L. Advances in quantum metrology. *Nature Photonics* **5**, 222–229 (2011).

[3] Huelga, S. F. *et al.* Improvement of frequency standards with quantum entanglement. *Physical Review Letters* **79**, 3865–3868 (1997).

[4] Sanders, B. C. Quantum dynamics of the nonlinear rotator and the effects of continual spin measurement. *Phys. Rev. A* **40**, 2417–2427 (1989).

[5] Dowling, J. P. Quantum optical metrology the lowdown on high-N00N states. *Contemporary Physics* **49**, 125–143 (2008).

[6] Greenberger, D. M., Horne, M. A. & Zeilinger, A. Going beyond bells theorem. In *Bells theorem, quantum theory and conceptions of the universe*, 69–72 (Springer, 1989).

[7] Knysh, S. I., Chen, E. H. & Durkin, G. A. True limits to precision via unique quantum probe. *arXiv preprint arXiv:1402.0495* (2014).

[8] Milburn, G., Corney, J., Wright, E. & Walls, D. Quantum dynamics of an atomic bose-einstein condensate in a double-well potential. *Physical Review A* **55**, 4318 (1997).

[9] Cirac, J., Lewenstein, M., Mølmer, K. & Zoller, P. Quantum superposition states of bose-einstein condensates. *Physical Review A* **57**, 1208 (1998).

[10] Mølmer, K. & Sørensen, A. Multiparticle entanglement of hot trapped ions. *Physical Review Letters* **82**, 1835 (1999).

[11] Orús, R., Dusuel, S. & Vidal, J. Equivalence of critical scaling laws for many-body entanglement in the lipkin-meshkov-glick model. *Physical review letters* **101**, 025701 (2008).

[12] Baumann, K., Guerlin, C., Brennecke, F. & Esslinger, T. Dicke quantum phase transition with a superfluid gas in an optical cavity. *Nature* **464**, 1301–1306 (2010).

[13] Skotiniotis, M., Sekatski, P. & Dür, W. Quantum metrology for the ising hamiltonian with transverse magnetic field. *New Journal of Physics* **17**, 073032 (2015).

[14] Liberti, G., Piperno, F. & Plastina, F. Finite-size behavior of quantum collective spin systems. *Physical Review A* **81**, 013818 (2010).

[15] Gammelmark, S. & Mølmer, K. Phase transitions and heisenberg limited metrology in an ising chain interacting with a single-mode cavity field. *New Journal of Physics* **13**, 053035 (2011).

[16] Law, C., Ng, H. & Leung, P. Coherent control of spin squeezing. *Physical Review A* **63**, 055601 (2001).

[17] Rojo, A. Optimally squeezed spin states. *Physical Review A* **68**, 013807 (2003).

[18] Scharf, G., Wreszinski, W., Hemmen, J. *et al.* Tunnelling of a large spin: mapping onto a particle problem. *Journal of Physics A: Mathematical and General* **20**, 4309 (1987).

[19] Garanin, D., Hidalgo, X. M. & Chudnovsky, E. Quantum-classical transition of the escape rate of a uniaxial spin system in an arbitrarily directed field. *Physical Review B* **57**, 13639 (1998).

[20] Ocak, S. B. & Altanhan, T. The effective potential of squeezed spin states. *Physics Letters A* **308**, 17–22 (2003).

[21] Ulyanov, V. & Zaslavskii, O. New methods in the theory of quantum spin systems. *Physics reports* **216**, 179–251 (1992).

[22] Sciolla, B. & Biroli, G. Dynamical transitions and quantum quenches in mean-field models. *Journal of Statistical Mechanics: Theory and Experiment* **2011**, P11003 (2011).

[23] Holstein, T. & Primakoff, H. Field dependence of the intrinsic domain magnetization of a ferromagnet. *Physical Review* **58**, 1098 (1940).

[24] Villain, J. Quantum theory of one-and two-dimensional ferro-and antiferromagnets with an easy magnetization plane. i. ideal 1-d or 2-d lattices without in-plane anisotropy. *Journal de Physique* **35**, 27–47 (1974).

[25] Hirsch, Jorge G and Castaños, Octavio and López-Peña, Ramón and Nahmad-Achar, Eduardo Virtues and limitations of the truncated Holstein–Primakoff description of quantum rotors. *Physica Script* **87**, 038106 (2013).

[26] Garg, A. Tunnel splittings for one-dimensional potential wells revisited. *American Journal of Physics* **68**, 430–437 (2000).

[27] Alhaidari, A. Solutions of the nonrelativistic wave equation with position-dependent effective mass. *Physical Review A* **66**, 042116 (2002).

[28] Jha, P. K., Eleuch, H. & Rostovtsev, Y. V. Analytical solution to position dependent mass schrödinger equation. *Journal of Modern Optics* **58**, 652–656 (2011).

[29] Zheng, S.-B. Quantum-information processing and multiatom-entanglement engineering with a thermal cavity. *Physical Review A* **66**, 060303 (2002).

[30] Robnik, M., Salasnich, L. & Vranicar, M. Wkb corrections to the energy splitting in double well potentials. *NONLINEAR PHENOMENA IN COMPLEX SYSTEMS-MINSK-* **2**, 49–62 (1999).

[31] Jiang, Z. Quantum fisher information for states in exponential form. *Physical Review A* **89**, 032128 (2014).

[32] Fujiwara, A. & Imai, H. A fibre bundle over manifolds of quantum channels and its application to quantum statistics. *Journal of Physics A: Mathematical and Theoretical* **41**, 255304–255304 (2008).

[33] Knysh, S., Smelyanskiy, V. N. & Durkin, G. A. Scaling laws for precision in quantum interferometry and the bifurcation landscape of the optimal state. *Physical Review A* **83** (2011).

[34] Javanainen, J. & Chen, H. Ground state of the double-well condensate for quantum metrology. *Physical Review A* **89**, 033613 (2014).

[35] Bardhan, B. R., Jiang, K. & Dowling, J. P. Effects of phase fluctuations on phase sensitivity and visibility of path-entangled photon fock states. *Physical Review A* **88**, 023857 (2013).

[36] Dorner, U. *et al.* Optimal quantum phase estimation. *Physical Review Letters* **102**, 040403 (2009).

[37] Van Dam, W., Mosca, M. & Vazirani, U. How powerful is adiabatic quantum computation? In *Foundations of Computer Science, 2001. Proceedings. 42nd IEEE Symposium on*, 279–287 (IEEE, 2001).

[38] Ulam-Orgikh, D. & Kitagawa, M. Spin squeezing and decoherence limit in ramsey spectroscopy. *Physical Review A* **64**, 052106 (2001).

[39] Ferrini, G., Spehner, D., Minguzzi, A. & Hekking, F. Effect of phase noise on quantum correlations in bose-josephson junctions. *Physical Review A* **84**, 043628 (2011).

[40] Johnson, M. *et al.* Quantum annealing with manufactured spins. *Nature* **473**, 194–198 (2011).

[41] Lanting, T. *et al.* Entanglement in a quantum annealing processor. *Physical Review X* **4**, 021041 (2014).

[42] Mølmer, K. & Sørensen, A. Risq-reduced instruction set quantum computers. *Journal of Modern Optics* **47**, 2515–2527 (2000).

[43] Gopalakrishnan, S., Lev, B. L. & Goldbart, P. M. Frustra-

tion and glassiness in spin models with cavity-mediated interactions. *Physical review letters* **107**, 277201 (2011).
[44] Torrontegui, E. *et al.* Shortcuts to adiabaticity. *Adv. At. Mol. Opt. Phys* **62**, 117–169 (2013).
[45] Berry, M. Transitionless quantum driving. *Journal of Physics A: Mathematical and Theoretical* **42**, 365303 (2009).
[46] Ulam-Orgikh, D. & Kitagawa, M. Spin squeezing and decoherence limit in ramsey spectroscopy. *Physical Review A* **64**, 052106 (2001).
[47] Ferrini, G., Spehner, D., Minguzzi, A. & Hekking, F. Effect of phase noise on quantum correlations in bose-josephson junctions. *Physical Review A* **84**, 043628 (2011).
[48] Ma, Jian & Wang, Xiaoguang & Sun, CP & Nori, Franco Quantum spin squeezing. *Physics Reports* **509**, 89–165 (2011).
[49] Chen, L., Aulbach, M. & Hajdušek, M. Comparison of different definitions of the geometric measure of entanglement. *Physical Review A* **89**, 042305 (2014).
[50] Barnett, S. M. & Radmore, P. M. *Methods in theoretical quantum optics*, vol. 15, chap. 3 (Oxford University Press, 2002).
[51] Paris, M. G. Quantum estimation for quantum technology. *International Journal of Quantum Information* **7**, 125–137 (2009).
[52] Tóth, G. & Apellaniz, I. Quantum metrology from a quantum information science perspective. *Journal of Physics A: Mathematical and Theoretical* **47**, 424006 (2014).
[53] Knysh, S. I. & Durkin, G. A. Estimation of phase and diffusion: combining quantum statistics and classical noise. *arXiv preprint arXiv:1307.0470* (2013).
[54] Barnett, S. M. & Pegg, D. Quantum theory of optical phase correlations. *Physical Review A* **42**, 6713 (1990).
[55] Macieszczak, K., Fraas, M. & Demkowicz-Dobrzański, R. Bayesian quantum frequency estimation in presence of collective dephasing. *New Journal of Physics* **16**, 113002 (2014).
[56] Personick, S. D. Application of quantum estimation theory to analog communication over quantum channels. *Information Theory, IEEE Transactions on* **17**, 240–246 (1971).
[57] Remembering $[y, \hat{P}] = i\delta$ and the inner derivatives: $[Q(y), \hat{P}] = i\delta \frac{dQ(y)}{dy}$ and $[R(\hat{P}), y] = -i\delta \frac{dR(\hat{P})}{d\hat{P}}$
[58] Assuming Γ is a Gaussian-distributed random variable of width σ, then a is also a random variable, but with a non-gaussian distribution $q(a) = p(a) \left|\frac{d\Gamma}{da}\right|$ that looks increasingly gaussian for $N \gg 1$ and fluctuations near the mean. The width in a is now approximately $\sigma g^{1/3}/18$. Remember the interesting range of $a \in [-4, 0]$ so the transverse field noise must be suppressed by a factor $N^{2/3}$ if the Goldilocks zone is to be located at all.

Appendix A: Variable-Mass Continuous Variable Ground State Compared with that of Discrete Spin System

Solutions to eqn.(5) are shown in FIG.8 for the ground (upper/red) and second excited state (lower/green) for the variable-mass particle in the one-dimensional potential $V(y)$ and different values of the annealing ratio $0 < \gamma < \infty$ (remembering the critical point is at $\gamma_c = 2$). Compared with the discrete ground state amplitudes ψ_m for the original quadratic spin Hamiltonian, good agreement is obtained. Fidelity to the original Hamiltonian eigenstates improves with larger ensembles and larger values of γ. For $\gamma \gtrsim 0$ the spin eigenstates contain discrete delta-like components (GHZ state) and the continuous approximation is no longer valid. Also, the continuous variable solution depends on the boundary conditions;

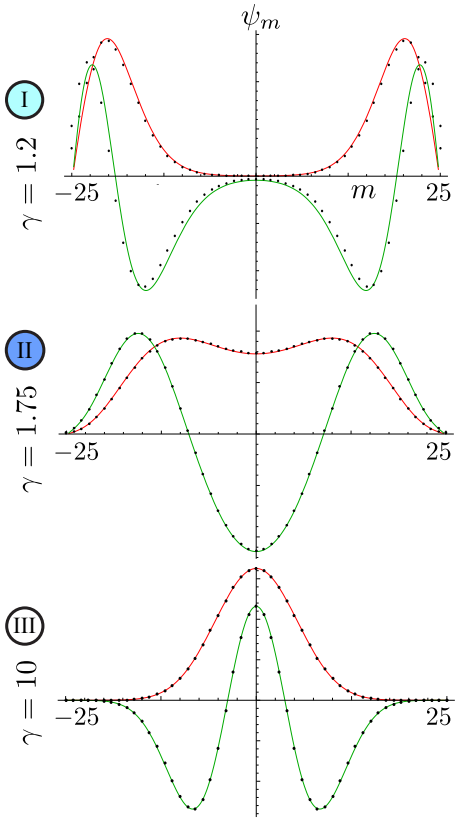

FIG. 8: Three annealing regions exist: (I) weak field, (II) critical field, and (III) strong field. Discrete ground state amplitudes and second excited state amplitudes for a system of 50 qubits ($N = 2j$) are indicated by black dots. The equivalent continuous wavefunction eigenstates for the variable-mass particle are shown by upper/red (ground state) and lower/green (second excited state) lines.

we have chosen $\psi(y) = 0$ at $y = \pm 1$ but the discrete amplitude set $\{\psi_m\}$ can be non-zero at $m = \pm j$ for finite j. An additional difference between the models is the discrete number of eigenstates for the spin system – in contrast, the particle model has no upper bound to the number of excited states.

Appendix B: Global Entanglement

Partial entanglement is necessary for probes to offer supra-classical precision in noisy interferometry. It will be a useful exercise, therefore, to quantify the entanglement present during the annealing process, in particular through the phase transition. To characterize entanglement a useful measure is the *global geometric entanglement* [49] (gge) which we can define for a pure entangled state $|\psi\rangle$ as:

$$\mathcal{G}[|\psi\rangle] = \min \left\{ -\log_2 |\langle \chi | \psi \rangle|^2 \right\} , \quad \forall\, |\chi\rangle \in S \qquad \text{(B1)}$$

i.e. where $|\chi\rangle$ belongs to the set of separable states S and the minimization is performed over all S. The function $\mathcal{G}$ is the negative logarithm of the fidelity of the entangled state to the nearest separable state. The nearest separable state will in

fact be a pure (product) state since the ground state is pure. The gge is sensitive to bipartite and multi-partite entanglement, although it does not differentiate between different entanglement depths.

For the current dynamics the spin ensemble lives in the maximum spin sector ($j_{\max} = N/2$), and therefore the ground state is fully permutation-symmetric. It is simple to argue that the nearest separable state also shares this permutation symmetry. If part of that state lived in a different j sector, an orthogonal subspace, it would only *reduce* the overlap $|\langle\chi|\psi\rangle|$. The only fully-symmetric pure separable states are in fact the spin-coherent states $|\chi\rangle \mapsto |\alpha,\beta\rangle$. Finding the gge can be a difficult optimization in general, but for symmetric states it means finding the optimal α,β angle pair – the polar and azimuthal angles of the spin vector giving maximum overlap with $|\psi\rangle$. The spin-coherent state[50] has components:

$$\langle m|\alpha,\beta\rangle = \left(\cos\frac{\alpha}{2}\right)^{2j}\sqrt{\binom{2j}{j+m}}\left(\mathrm{e}^{-i\beta}\tan\frac{\alpha}{2}\right)^{j+m} \tag{B2}$$

The ground state of the quadratic spin system has real coefficients, as does the closest spin coherent state: $\beta = 0$. Also the probability distribution $|\langle m|\alpha,\beta\rangle|^2$ is binomial, with mean $\langle\hat{J}_z\rangle = j\cos\alpha$ and variance $(\Delta\hat{J}_z)^2 = (j/2)\sin^2\alpha$. Approximating the binomial distribution as Gaussian in the $j \gg 1$ limit and converting to y produces a mean $y_\alpha = \cos\alpha$ and standard deviation $\sigma_\alpha = j^{-1/2}|\sin\alpha|$. Obviously $\sigma_\alpha \leq j^{-1/2}$ is the upper bound on wavefunction 'width' for a separable state.

In Region III the ground state is centered on $y = 0$ and the nearest spin-coherent state will also be centered on the origin, being as wide as possible, i.e. $\alpha = \pi/2$. The squared overlap of two Gaussian wavefunctions with the same mean but different variances is $2\sigma_a\sigma_b/(\sigma_a^2+\sigma_b^2)$. The gge for $\Gamma > \Gamma_c$ is then:

$$\mathcal{G} = \log_2\left[(3-2/\Gamma)^{1/4} + (3-2/\Gamma)^{-1/4}\right] - 1 \tag{B3}$$

As we have seen, the ground-state passing into Region I during an annealing cycle bifurcates into two approximately Gaussian lobes. The nearest spin-coherent state will choose one of those lobes and attempt to match both its mean and variance (to achieve maximum fidelity). Interestingly, an almost exact matching for both quantities is possible although the spin coherent state is a function of a single parameter α. The bi-modal lobes of the ground state have means $\pm y_0 = \pm\sqrt{1-1/M_\gamma^2}$ and standard deviation $\sqrt{1/y_0 - y_0}$. Fidelity to the spin-coherent state, with y_α and σ_α given above, can be close to unity only if:

$$\alpha_{\text{opt}} = \arctan\left[\frac{\sqrt{M_\gamma}}{(M_\gamma^2-1)^{3/4}}\right], \quad 0 < \gamma < 2 \tag{B4}$$

remembering that $M_\gamma = 2/\gamma = 2\Gamma/(1-\Gamma)$. This gives an asymptotic result for the entanglement in terms of the variable mass:

$$\mathcal{G} = \log_2\left[\left(1-1/M_\gamma^2\right)^{1/4} + \left(1-1/M_\gamma^2\right)^{-1/4}\right] \tag{B5}$$

valid in the parameter range, $\Gamma < \Gamma_c$. Only half the probability (with some exponentially small correction) is concentrated in a single lobe, so the overall fidelity to the ground state will quickly converge on $1/\sqrt{2}$ in Region I. Then $\mathcal{G} \sim 1$, which is the known gge for a GHZ state, a state with *only* N-partite entanglement. This analysis also indicates how well-conceived is the model of a 'cat' state with two superposed spin-coherent states, for this spin Hamiltonian and $\Gamma < \Gamma_c$, as presented in Ref. 9.

In the scale-free setting of FIG.9 it is seen that for $N = 100$ qubits the maximum global entanglement is at $a_G \approx -3.85414$. For larger N or j this maximum will therefore occur in the region $a_G < a < 0$ because of the properties of the nearest spin-coherent state. In the y variable this state has width $1/\sqrt{j}$ but in the scale-free variable $z = yg^{1/6} \propto yj^{1/3}$, the maximum width becomes $j^{-1/6}$. The squared overlap of the widest spin-coherent state with the ground state in Region II (whose variance is just a pure number in the z-variable near critical annealing) is going to scale asymptotically as $\propto 1/j^{1/6}$ or $1/N^{1/6}$. The gge in the limit $N \gg 1$ therefore approaches:

$$\mathcal{G}_\infty \sim \frac{1}{6}\log_2 N \tag{B6}$$

which confirms the central result of Ref.11 for the (isotropic) Lipkin-Meshkov-Glick model. Note that the entanglement per copy vanishes in the thermodynamic limit, as $(\log N)/N \sim 0$. We should not be too shocked by this scaling law as it has been shown that although in general $\mathcal{G} < N-1$, the maximum entanglement for *symmetric* states is $\mathcal{G}_\infty \sim \log_2(N+1)$.

Appendix C: Calculating Quantum Fisher Information

Consider a phase parameter θ encoded by a spin Hamiltonian, e.g. $\hat{J}_z$ aligned with the spatial z direction, acting on a noisy mixed quantum state ρ, of N qubits. Assume the noise process commutes with the phase rotation, as is the case e.g. dissipation and for collective dephasing. The mixed state is transformed by $\exp\{-i\theta\hat{J}_z\}$ and for such finite-dimensional systems the calculation of QFI typically involves diagonalization of the density matrix [51, 52]. For $\rho(\theta) = \sum_i \lambda_i|\psi_i\rangle\langle\psi_i|$ then defining the QFI as $F(\theta)$, it is:

$$2\sum_{i,j}\frac{|\langle|\psi_i|\rho'(\theta)|\psi_j\rangle|^2}{\lambda_i+\lambda_j} \mapsto 2\sum_{i,j}\frac{(\lambda_i-\lambda_j)^2}{\lambda_i+\lambda_j}\left|\langle\psi_i|\hat{J}_z|\psi_j\rangle\right|^2 \tag{C1}$$

where $\rho'(\theta) = d\rho/d\theta$. The computation becomes increasingly arduous for $N \gg 1$ without introducing any insight into the result. Recently, a different formulation was proposed, useful in the large N case, where $F(\theta)$ may be expanded as an exact asymptotic series [31, 53]:

$$F = \left\langle\left[\hat{J}_z, 2\tanh\left(\frac{1}{2}\left[-\log(\rho), \bullet\right]\right)\hat{J}_z\right]\right\rangle . \tag{C2}$$

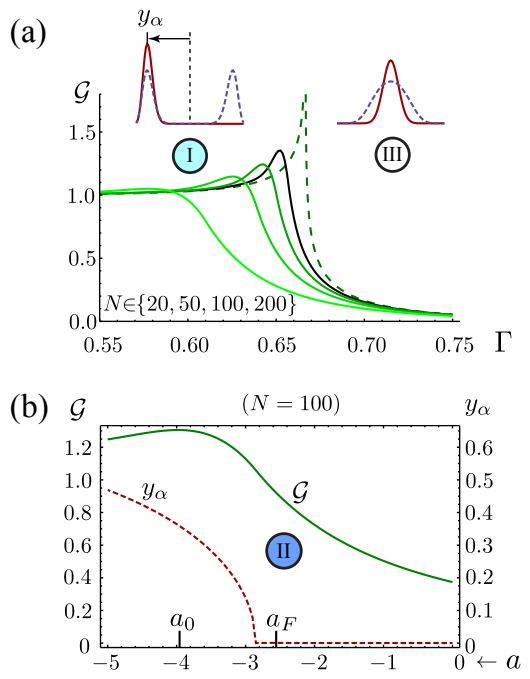

FIG. 9: Global Entanglement: Upper plot (a) shows the analytic bounds on global geometric entanglement $\mathcal{G}$ in the thermodynamic limit (dashed green curve) as a function of Γ. The unbroken green curves depict the entanglement for finite sized ensembles up to $N = 200$ (black curve). The superimposed red and (dotted) blue distributions show the amplitudes of the nearest spin-coherent state (red) to the ground state of the annealed system (blue/dotted) in the original spin problem. This spin-coherent state is also the nearest (or highest fidelity) separable state. Finding this state is crucial, due to $\mathcal{G}$ being the negative logarithm of the square of the overlap between these two states. When the ground state centered on $y = 0$ bifurcates into two lobes as it passes from Region III to Region I the nearest spin-coherent state (having an approximately Gaussian distribution) can only track one of the lobes; its mean $y_\alpha = \cos\alpha$ starts to move with decreasing $\Gamma < 2/3$. As Γ approaches 0 the entanglement asymptotes to $\mathcal{G} = 1$, the entanglement of a GHZ state. The lower graph (b) plots the entanglement $\mathcal{G}$ more closely in Region II for a system of $N = 100$ qubits in the scale-free setting. Maximum entanglement is seen to occur in the vicinity of the minimum gap, but this maximum will be closer to $a = 0$ or $\Gamma = \Gamma_c$ for larger N. As N increases the maximum width of a spin-coherent state scales as $N^{-1/6}$ in the z variable. Thus maximum entanglement grows slowly as $\frac{1}{6}\log N$. The red dotted curve plots the locus of the mean y_α of the nearest spin-coherent state. Apparently, as a or Γ decreases the ground state has already begun to bifurcate before maximum entanglement is reached.

Here square brackets denote an operator commutator, $[A, B] = AB - BA$, and angular brackets indicate an expectation value taken with the density matrix, $\langle\hat{A}\rangle = \mathrm{Tr}(\rho\hat{A})$. The adjoint endomorphism $[A, \bullet] = \mathrm{ad}_A$ acts as a superoperator. Thus $[A, \bullet]\hat{J}_z = [A, \hat{J}_z]$, and $[A, \bullet]^3\hat{J}_z = [A[A, [A, \hat{J}_z]]]$ are terms in the power series expansion of the hyperbolic tangent; $\tanh x = x - x^3/3 + \ldots$ with $x = [A, \bullet]$, and acting on the $\hat{J}_z$ total spin operator. This series expression (C2) provides the leading terms in the formulation of the QFI as an action[53] in eqn.(16).

Appendix D: Decoherence function μ

For pure collective dephasing, (background phase fluctuations with variance κ^0, possibly due to stochastic path length fluctuations inside the interferometer), this becomes a constant $\mu(y) \mapsto \mu_0 = N^2\kappa^0$ within the physical box boundary $y = m/j \in [-1, 1]$ and infinite outside the boundary. This collective dephasing is the most significant type of noise for a Bose-Einstein condensate, existing only in the fully symmetric subspace of its constituent atoms, although losses may also occur as atoms leave the condensate. Likewise, along with losses, collective dephasing is a dominant noise source in photonic interferometry. The dephasing process can be seen as a convolution of a pure probe state $|\psi\rangle$ with a Gaussian probability distribution $p_G(\theta, \bar{\theta}, \kappa^0) = \exp\{-(\theta - \bar{\theta})^2/2\kappa^0\}/\sqrt{2\pi\kappa^0}$ with mean $\bar{\theta}$ and variance κ^0:

$$\rho = \int_{2\pi} p_G(\theta, \bar{\theta}, \kappa^0)\ |\psi(\theta)\rangle\langle\psi(\theta)|\ \mathrm{d}\theta\ . \tag{D1}$$

The density matrix is a mixture of these probes, each evolved by a different phase: $|\psi(\theta)\rangle = \exp\{-i\hat{J}_z\theta\}|\psi(0)\rangle$. The analysis also requires that $\kappa^0 \ll 1$. For strong phase noise beyond this limit the stochastic phase distribution can no longer be approximately Gaussian and localized within a 2π window; periodic boundary conditions turn the random phase distribution into a wrapped normal distribution. By then, any probe state is so noisy it becomes almost completely insensitive to phase, and precision begins to decay exponentially fast in κ^0 (due to the phase uncertainty relation[7, 54]) . There are now two bounds on our analysis. Including the requirement that the noise parameter $\kappa^0 N^2$ is large, so that the asymptotic series can be truncated:

$$1/N \ll \sqrt{\kappa^0} \ll 1\ . \tag{D2}$$

Collective dephasing is also important in a Bayesian estimation scheme, featuring a prior phase distribution that is updated via measurements. Dephasing is entirely equivalent to Gaussian-distributed *prior* phase uncertainty[55, 56] $\Delta\theta = \sqrt{\kappa^0}$. In general, there will always be some prior phase uncertainty (estimation would be otherwise be unnecessary) and thus collective phase noise is always present

Adding local noise $\kappa^{(L)} = \mathrm{e}^\zeta - 1$ while the interferometric phase θ is being acquired is governed by a Markovian master equation:

$$\frac{d\rho}{d\theta} = -i[\hat{J}_z, \rho]\ +\ \frac{d\zeta}{d\theta}\sum_{i=1}^{N}\mathcal{L}_s^{(i)}\rho \tag{D3a}$$

$$\mathcal{L}_s(\rho) = \{\hat{s}^\dagger\hat{s}, \rho\} - 2\hat{s}\rho\hat{s}^\dagger \tag{D3b}$$

(the latter expression defines the Linbladian sueroperator $\mathcal{L}$). Possible noise processes are local dephasing in the interferometric phase basis $\hat{s} \mapsto \frac{1}{2}\hat{\sigma}_z$, excitation $\hat{s} \mapsto \frac{1}{2}\hat{\sigma}^+$ and relaxation $\hat{s} \mapsto \frac{1}{2}\hat{\sigma}^-$ defined in terms of individual Pauli spin

operators. Other noise processes are plausible, e.g. transverse dephasing $\hat{s} \mapsto \frac{1}{2}\hat{\sigma}_x$, but this is much less deleterious to precision, and its slight influence will be swamped by the z-basis noise for $N \gg 1$. Note that $\sum_{i=1}^{N} \frac{1}{2}\hat{\sigma}_z^{(i)} = \hat{J}_z$. In the current analysis all qubits are permutation-invariant and decohere at the same rate; there are no topological features to this model. Including local noise, the noise parameter μ_0 becomes a function of the $y = m/j$ spin projection variable,

$$\mu(y) = N^2\kappa^0 + N\kappa^{(L)}/(1-y^2) \; , \tag{D4}$$

with more details in Ref. [7]. It was also shown there that for local noise only the combination of dephasing, relaxation and excitation included in $\kappa^{(L)} = \mathrm{e}^{\zeta} - 1$ matters asymptotically, not their individual contributions:

$$\zeta = \zeta_z + \zeta_- + \zeta_+ \; . \tag{D5}$$

In this paper, we considered the hybrid noise function $\mu(y)$ in the general form given above.